# Radio-Frequency Flexible and Stretchable Electronics: The Need, Challenges and Opportunities

Yei Hwan Jung[a], Jung-Hun Seo[b], Huilong Zhang[a], Juhwan Lee[a], Sang June Cho[a], Tzu-Hsuan Chang[a], Zhenqiang Ma*[a]

[a]Dept. of Electrical and Computer Engineering, University of Wisconsin-Madison, WI USA 53705;
[b]Dept. of Materials Design and Innovation, University of Buffalo, Buffalo NY USA 14228

*mazq@engr.wisc.edu; phone 1 (608) 261-1095

## ABSTRACT

Successful integration of ultrathin flexible or stretchable systems with new applications, such as medical devices and biodegradable electronics, have intrigued many researchers and industries around the globe to seek materials and processes to create high-performance, non-invasive and cost-effective electronics to match those of state-of-the-art devices. Nevertheless, the crucial concept of transmitting data or power wirelessly for such unconventional devices has been difficult to realize due to limitations of radio-frequency (RF) electronics in individual components that form a wireless circuitry, such as antenna, transmission line, active devices, passive devices etc. To overcome such challenges, these components must be developed in a step-by-step manner, as each component faces a number of different challenges in ultrathin formats. Here, we report on materials and design considerations for fabricating flexible and stretchable electronics systems that operate in the microwave level. High-speed flexible active devices, including cost effective Si-based strained MOSFETs, GaAs-based HBTs and GaN-based HEMTs, performing at multi-gigahertz frequencies are presented. Furthermore, flexible or stretchable passive devices, including capacitors, inductors and transmission lines that are vital parts of a microwave circuitry are also demonstrated. We also present unique applications using the presented flexible or stretchable RF components, including wearable RF electronics and biodegradable RF electronics, which were impossible to achieve using conventional rigid, wafer-based technology. Further opportunities like implantable systems exist utilizing such ultrathin RF components, which are discussed in this report as well.

**Keywords:** Flexible Electronics, Stretchable Electronics, Radio-Frequency, Microwave Electronics, High-Frequency

## 1. INTRODUCTION

Many years ago, fabricating electronic devices that can bend or stretch could only be realized using organic semiconductors with soft moduli. Now, bendable devices using conventional inorganic semiconductors are readily introduced to create flexible and stretchable electronics with comparable performances to state-of-the-art electronics [1]. Transfer printing techniques have evolved to create electronic devices on nearly any type of substrates, including biodegradable papers and ultrathin biocompatible films [2-4]. These unusual format electronics enabled new applications that were impossible to address with conventional rigid electronics. To extend the capabilities of the applications, radio frequency electronics must be implemented for wireless function of flexible and stretchable electronics. Radio frequency devices require high mobility semiconductors and high quality dielectric materials for maximum speed and power gain. In addition, microfabrication techniques must be pushed to the limits to create extremely small feature sizes and thin films, which then, can only operate at high frequencies [5]. Such advanced fabrication and materials engineering requirements propose significant challenges on bendable or stretchable unconventional substrates like plastic and rubber. In this report, we review the past efforts made from our research group to create high-frequency devices on such substrates and introduce some of the emerging technologies on how they may be utilized for future generation of flexible and stretchable electronics. As a fully functional microwave integrated circuit requires both active and passive components, both efforts were made in parallel to achieve this goal. The complete set of devices presented here can form basic elements in microwave engineering on flexible or stretchable substrates.

# 2. HIGH-SPEED ACTIVE DEVICES

## 2.1 Silicon-based high-speed flexible MOSFETs

Si is the most widely used conventional material for electronics, as it is abundant and has descent intrinsic properties required for high-performance electronics. Although it is less utilized for high-frequency applications, Si can be tweaked to boost intrinsic properties to be useful as a high-frequency device [6]. For the Si based devices, further improvement of device speed implies significant technical and economic advantages. While the mobility of bulk Si can be routinely enhanced using strain techniques, implementing these techniques into transferrable single-crystalline Si nanomembranes (NM) for fast flexible electronics has been challenging and not demonstrated. Here we demonstrate the combination of self-sustained strain sharing with strained- NM compatible doping techniques to create strained, print-transferrable Si
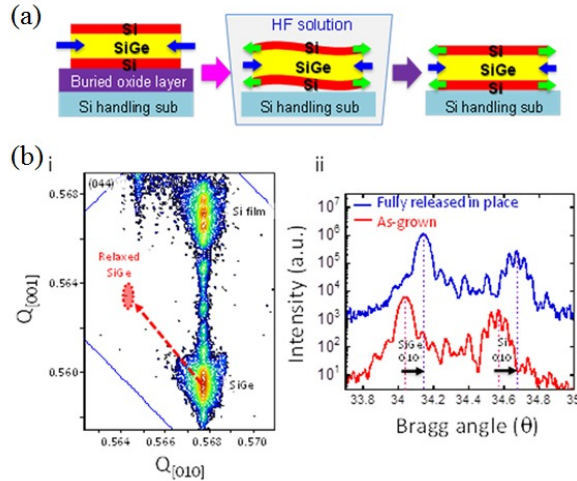


Figure 1. (a) Process flow to implement the strain sharing using Si/SiGe/Si epitaxial trilayer structure. (b) X-ray diffraction before and after release of the trilayer NM. i, On-axis line scan around the (004) reflection before and after release of the trilayer NM. ii, Off-axis RSM around the (044) reflection for the as-grown trilayer structure. Adapted from [7].
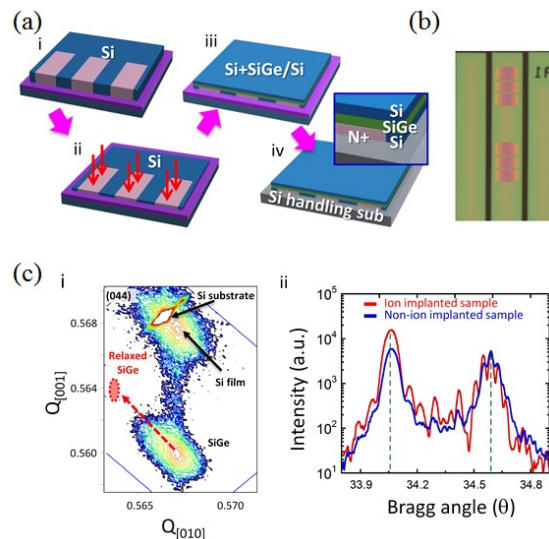


Figure 2. (a) Doping of strained trilayer structure. (b) Image of doped strained NM after transferring to a plastic substrate. (c) XRD of as-grown ion-implanted trilayer NM. i. Off-axis RSM around the (044) reflection. ii. On-axis line scans around the (004) reflection comparing the doped and undoped as-grown trilayer NMs. Adapted from [7].

NMs [7]. The combination led us to demonstrate a new speed record of Si based flexible electronics without using aggressively scaled critical device dimensions. Figure 1(a) illustrates the strain sharing techniques. Creation of self-sustained strain in Si NMs started from growing 80 nm of undoped $Si_{0.795}Ge_{0.205}$ epitaxial layer on silicon-on-insulator (SOI) wafer with a thin-downed 48 nm top Si layer. A nearly symmetrical trilayer structure (Si/SiGe/Si) was formed by growing 46 nm of undoped Si on top of the SiGe. Due to the lattice mismatch between Si and SiGe, the SiGe layer in the trilayer structure was compressively strained to the Si in-plane lattice constant (mismatch strain, $\varepsilon_m$ = -0.77%). The trilayer NM was released by selective removal of the $SiO_2$ (BOX) layer of the SOI. During the release, strain sharing occured between the SiGe and Si layers. To demonstrate the effectiveness of the self-sustained straining approach, Figure 1(b)(i) shows an X-ray diffraction (XRD) off-axis reciprocal-space map (RSM) around the (044) reflection for the as-grown trilayer structure. The RSM indicates that the SiGe layer was strained to the Si lattice constant; the Si and SiGe peaks lied along the same vertical line. This result confirms that there was no plastic relaxation of the mismatch strain in the alloy before release of the trilayer. To realize high device speed, the NMs must be properly doped. We designed an alternative approach by applying the ion implantation and anneal processes to an unstrained Si layer on SOI as shown in Figure 2(a) and (b). The doping and thinning down procedures have some effect on the crystallinity of the as-grown Si/SiGe/Si trilayers by a general broadening of the diffraction peaks in Figure 2(c).

Figure 3(a) shows the transfer curve and transconductance ($g_m$) versus gate voltage ($V_g$) of a strained-channel TFT along with the results measured from the unstrained-channel TFT for comparison. The highest $g_m$ for the strained TFTs was 386 µS. Comparing to the unstrained reference TFTs with identical dimensions, the 47.3% enhancement of the peak $g_m$ values in the strained TFT was observed and is mainly ascribed to mobility enhancement, which is due to the introduction of the tensile strain in the Si channel of the trilayer. The $g_m$ and mobility enhancement ratios were consistent with the expected value. Figure 3(b) plots the $g_m$ versus drain current. Figure 3(c) and (d) show the measured current gain ($H_{21}$) and power gain ($G_{max}$) of the strained TFT, indicating that the cut-off frequency ($f_T$) is 5.1 GHz and the maximum oscillation frequency ($f_{max}$) is 15.1 GHz.
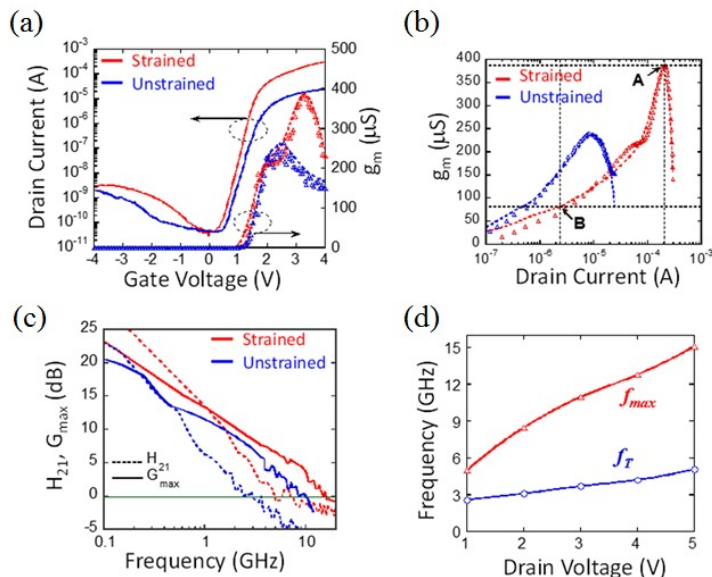
## 2.2 GaAs-based high-speed flexible HBTs



Figure 3. (a) Transfer curves and transconductance ($g_m$) curves of unstrained and strained devices ($V_{ds}$ = 50mV). (b) $g_m$ is plotted as a function of drain current. Point A indicates the peak $g_m$ where peak $f_T/f_{max}$ were measured. Point B is where 3.5GHz $f_{max}$ can be obtained. (c) Current gain ($H_{21}$) and power gain ($G_{max}$) as a function of frequency of unstrained and strained devices ($V_g$=4V, $V_{ds}$=5V). (d) $f_T$ and $f_{max}$ of strained devices as a function of drain bias under fixed gate bias ($V_g$=4V). Adapted from [7].

GaAs based HBTs and Schottky diodes have been fabricated for flexible RF applications on flexible cellulose nanofiber (CNF) substrate [3]. The fabrication of GaAs HBT started with conventional non-self-aligned GaAs HBT fabrication process on GaAs wafer with AlGaAs sacrificial layer. A thick layer of photoresist (~ 7 μm) was used as anchor for holding and protecting GaAs HBTs during undercut process, in which the device was undercut etched in diluted hydrofluoric (HF) solution (1:100) for 3 hours. After the fully undercut, the GaAs HBT was transferred onto a temporary substrate with a thin layer of polyimide (PI) and poly(methyl methacrylate) (PMMA) on a Si substrate. Then, another layer of PI was spin casted on the GaAs HBT on temporary substrate as encapsulating layer. After via opening, ground-signal-ground RF pads were deposited on the device for characterization later. The PMMA sacrificial layer of PI encapsulated device was undercut etched in hot acetone. Following fully dissolving PMMA, the device was picked up by PDMS elastomer stamp and transferred onto the CNF substrate which had a layer of SU-8 as adhesive. Figure 4(a) shows GaAs HBT on CNF substrate on a tree leaf. DC characterization of the GaAs HBT on CNF substrate shows highest gain (β) of 14.49 when $V_{BE}$ was biased at 1.86 V, as shown in Figure 4(b). Scattering (S-) parameters measurement of GaAs HBT was conducted with bias of $V_C = 2$ V and $I_B = 2$ mA to characterize RF performance of GaAs HBT. After de-embedding the parasitic effects using short and open pattern on same substrate, the current gain ($H_{21}$) and power gain ($G_{MAX}$) of the GaAs HBT are demonstrated in Figure 4(c). The GaAs HBT can achieve cut-off frequency ($f_T$) of 37.5 GHz and maximum oscillation frequency ($f_{max}$) of 6.9 GHz. The relatively low $f_{max}$ is caused by the non-self-aligned structure. The 2 μm emitter to base spacing resulted from high base resistance, which diminished the $f_{max}$. This GaAs HBT is capable of working in GSM and Wi-Fi channel, which is in the range of 800 to 2500 MHz. Schottky diodes based on GaAs were also fabricated in similar way as the GaAs HBT. The current-voltage measurement in Figure 4(d) shows good ideality factor of 1.058 and low turn-on voltage of 0.7 V. S-parameters of GaAs Schottky diode demonstrated in Figure 4(e) and (f) show the RF performance of the device at forward current bias of 10 mA and reverse voltage bias of -0.5 V, respectively. The insertion loss ($S_{21}$) was only -1 dB at 20 GHz under forward bias and -2 dB at 4.3 GHz, which presents potential for microwave switching applications. A full bridge rectifier using GaAs Schottky diodes and metal-insulator-metal (MIM) capacitor was fabricated on CNF substrate, as shown in Figure 4(g). The rectification behavior was measured using an input RF signal at 5.8 GHz. With increasing RF input power, the DC
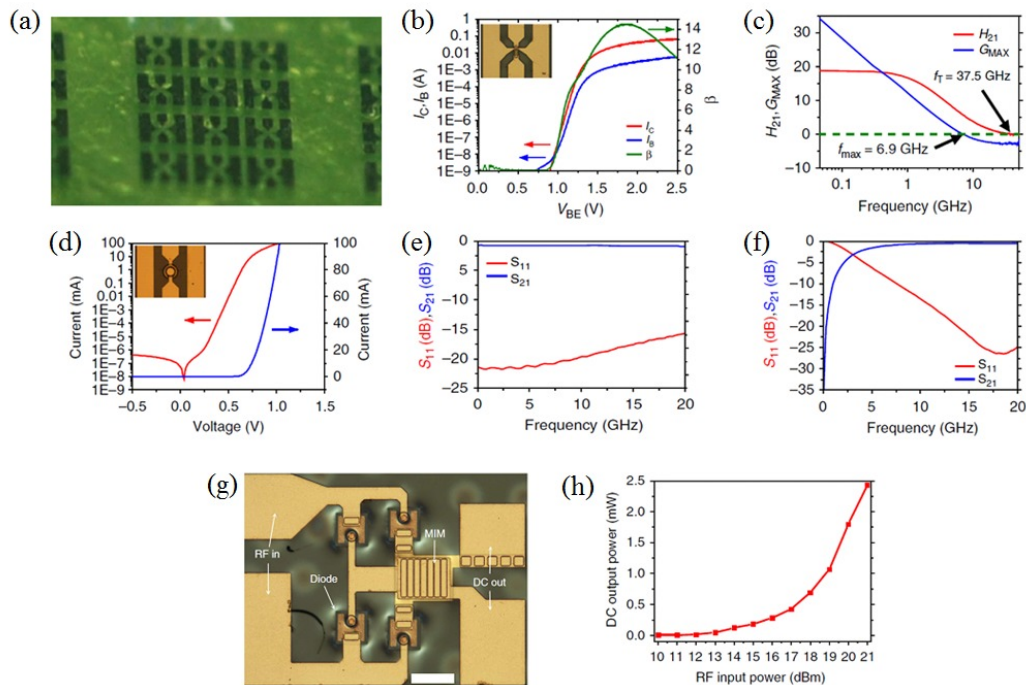


Figure 4. (a) Photograph of an array of HBTs on CNF substrate on a tree leaf. (b) Gummel plot and gain (β) of GaAs HBT (inset, optical image of a GaAs HBT). (c) Current gain and power gain as a function of frequency. (d) Current-Voltage curve of GaAs Schottky diode (inset, optical image of a GaAs Schottky diode). (e) S-parameters ($S_{11}$ and $S_{21}$) of GaAs Schottky diode under forward current bias of 10 mA. (f) S-parameters ($S_{11}$ and $S_{21}$) of GaAs Schottky diode under reverse voltage bias of -0.5 V. (g) Optical image of a full bridge rectifier on CNF substrate. (h) DC output power of the rectifier as a function of RF input power. Adapted from [9].

output power could achieve 2.43 mW output power with input power of 21 dBm as shown in Figure 3(h). Among the compound semiconductors, GaAs is the most widely used material in electronics as more than 85% of today's consumer electronics with wireless communication capabilities, such as cell phones and mobile tablets, employ GaAs-based microwave devices for their superior high-frequency operation and power handling capabilities. The thin film GaAs devices obtained using this method would not only save the expensive material, but also allow mobile devices in flexible formats.

## 2.3 GaN-based high-speed flexible HEMTs

While Si- or GaAs- based transistors may be the suitable choice for high speed flexible applications, GaN-based high electron mobility transistors (HEMTs) have achieved one-order magnitude higher power density and power conversion efficiency compared to the competing technologies. Considering the low thermal dissipation coefficient of the general flexible materials, GaN based transistors with best conversion efficiency are the best candidate for the high power flexible amplifiers. To effectively embed the thin film GaN HEMTs on the flexible substrate, as shown in Figure 5a, we have transferred the thin film AlGaN/GaN HEMTs on a plastic substrate by selectively removing the growth substrate through $XeF_2$ gas phase etching. Figure 5b shows the large scale, highly transparent, 8×8 mm GaN NM transferred on a plastic substrate. The pre-fabricated GaN HEMTs on the transferred GaN membrane, as presented in Figure 5c, demonstrated good DC properties, as shown in Figure 5c and Figure 5d, and measured with high frequency response ($f_T/f_{max}$ = 50/115 GHz). Large scale flexible GaN nanomembrane features good thermal properties on the flexible film [8], and the same technique can be utilized to achieve the stretchable GaN HEMTs and hence the stretchable power amplifiers. In Figure 6a, the stretchable power transistors are combined with the pre-defined circular-
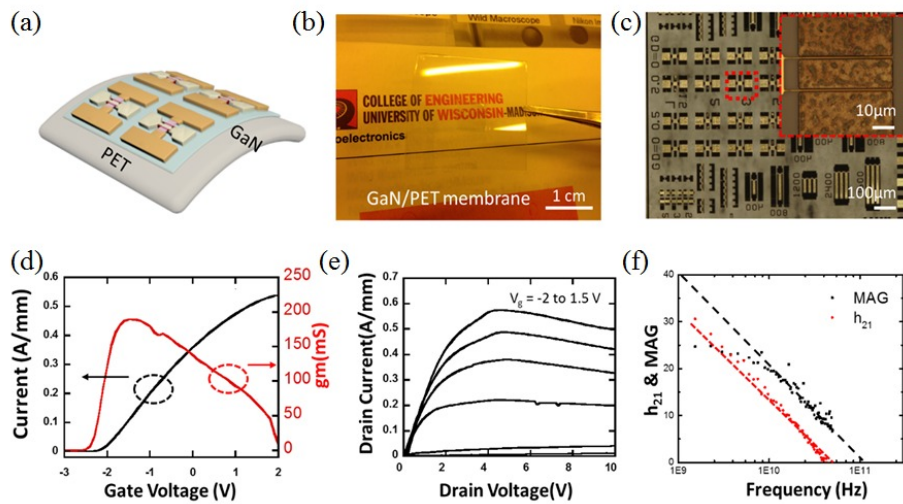


Figure 5. High speed transparent and flexible AlGaN/GaN HEMTs on PET film. (a) Schematic of the flexible AlGaN HEMTs transferred on PET film. (b) Optical image of transferred 8mm×8mm GaN nanomembrane on PET film. (c) AlGaN/GaN HEMTs with gate length 400nm. DC characteristics of (a) Id-Vg, (b) Id-Vd, and (c) RF characteristics including $h_{21}$ and MAG. Adapted from [8].
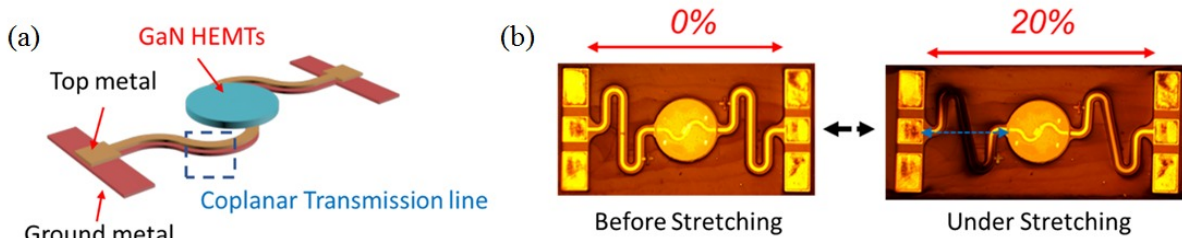


Figure 6. High Speed stretchable AlGaN/GaN HEMTs with coplanar transmission. (a) Schematic of the stretchable AlGaN HEMTs (b) Stretchable AlGaN/GaN under 0% and 20% strain.

shaped GaN NM and low-loss stretchable coplanar transmission line. The embedded GaN HEMTs transferred on Dupont plastic tape demonstrated high stretchability under applied strain. The stretchable/flexible GaN HEMTs demonstrated here can form the route to design capabilities of next generation high performance flexible electronics for a variety of applications.

## 3. HIGH-SPEED PASSIVE DEVICES

### 3.1 Flexible capacitors, inductors and filters

RF circuits use spiral inductors and metal-insulator-metal (MIM) capacitors as matching components between RF blocks. Like conventional CMOS and MMIC technology, the passive components such as spiral inductors and MIM capacitors need to have their own library to adapt with various dielectric constants of flexible substrates. In conjunction with flexible active devices, many authors researched both robust and mechanically bendable, high frequency passive components such as inductors and capacitors. Numerous types of filters with various combinations of flexible inductors and capacitors were also demonstrated for a more complex matching. The first inductors and capacitors demonstrated on flexible substrates could achieve high-frequency under bending conditions [9]. However, the self-resonance frequency ($f_{res}$) of these inductors and capacitors were limited by 9.1 GHz and 13.5 GHz, respectively. Optimizing the materials and fabrication processes, enhanced versions of such passive devices were demonstrated with capabilities reaching X-band (8 to 12 GHz) operation, as shown in Figure 7 [10]. Finally, passive components that could reach Ku-band (12 to 18 GHz) operation, including filters were demonstrated, as presented in Figure 8(a)-(d) with optimized designd and fabrication processes [11]. The self-resonance frequency of inductors and capacitors optimized here showed 19.1 GHz and 25.4 GHz, respectively. It also combined its high $f_{res}$ lumped flexible inductors and capacitors to make band pass filters in Figure 8(e) and notch filters in Figure 8(f). These filters are represented by optical image in Figure 8(g). The device is ultrathin that it can be laminated on a fingernail as demonstrated in Figure 8(h). The flexible series and parallel resonance lumped circuits can be implemented with high speed active components for microwave integrated circuit.

### 3.2 Stretchable transmission lines

Current technologies for stretchable electrodes have been utilizing different types of serpentine designs to enhance intimate fabrication of wearable electronics onto skin [12, 13]. However, studies on those stretchable interconnects were limited to designs primarily for electrical operation at direct current (DC) signals or alternating current (AC) signals at very low frequency that is typically less than 1 GHz. As the working frequency of current wireless communication system increases to higher frequency (RF) level (i.e. multi-gigahertz), it is necessary to develop essential elements including active and passive elements of microwave circuit as a form of soft, flexible, or stretchable component which is still in compliance with conventional microwave circuit technology. Therefore, underlying studies on passive elements
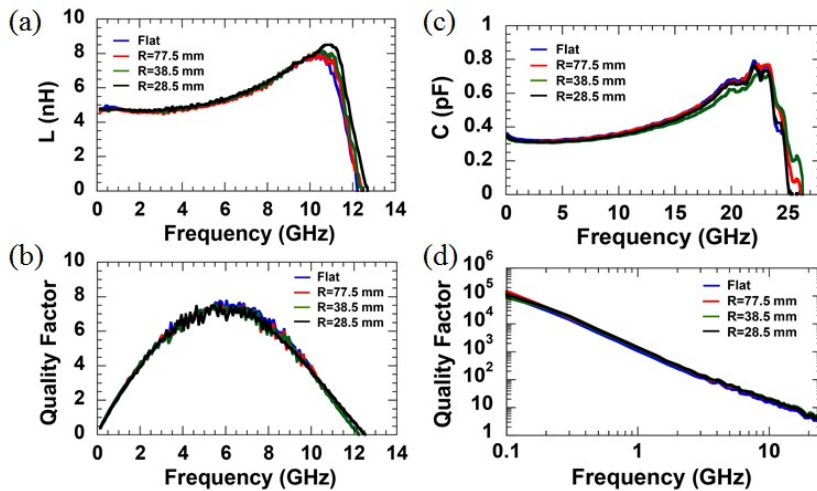


Figure 7. Measured 4.5 turns spiral inductors with 4.5 turns, 20 μm line width, and 4 μm line space. (a) L values and (b) Q values as a function of frequency under flat and various bending states. Measured (c) capacitance values and (d) Q values of an 88 x 88 μm$^2$ MIM capacitor as a function of frequency under flat and bending conditions. Adapted from [10].

such as stretchable RF transmission lines are mandatory and innovative design consideration becomes crucial.

The stretchable RF transmission line can have unique twisted-pair design integrated into serpentine microstructure [14]. It can minimize electromagnetic interference from surrounding area, such that the transmission line is minimally
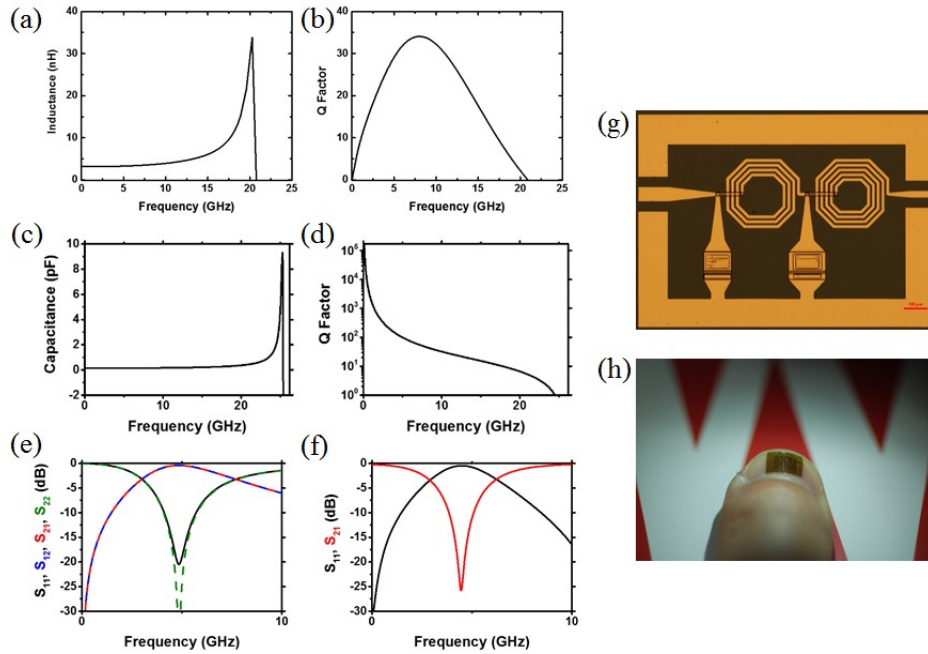


Figure 8. (a) Inductance against frequency and (b) Q factor of a 2.5 turn spiral inductor. (c) Capacitance against frequency and (d) Q factor of a 40 μm × 40 μm large MIM capacitor. S-parameters plotted against frequency for (e) a 4.8 GHz band pass filter and (f) 4.5 GHz notch filter. (g) Optical microscopy image of the flexible low pass filter. (h) Ultrathin passive devices coated on a fingernail. Adapted from [11].
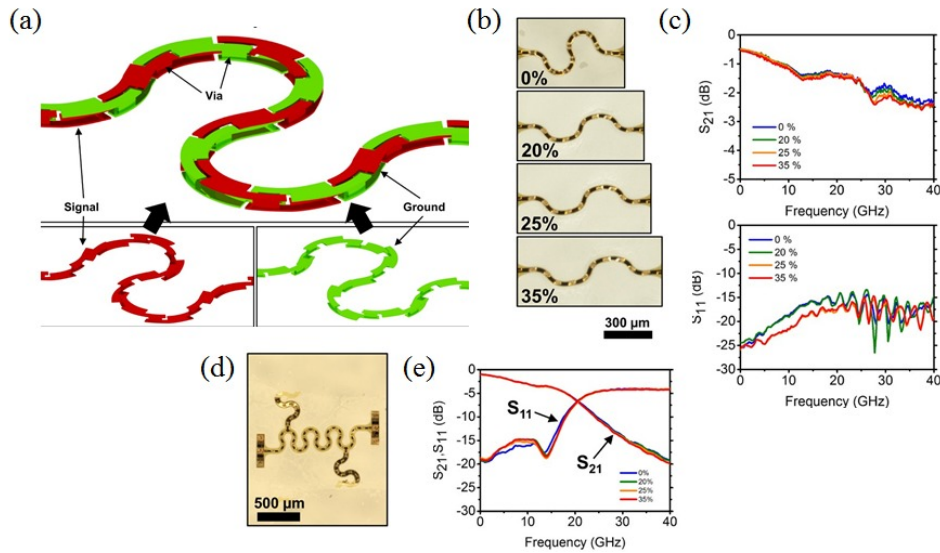


Figure 9. (a) The concept of twisted-pair-based stretchable transmission line. (b) Optical microscopy image of the stretchable transmission line with 0%, 20%, 25%, and 35% elongation (c) Measured $S_{21}$ and $S_{11}$ of the stretchable transmission line with two turns of serpentine at 0%, 20%, 25%, and 35% elongation plotted against frequency. (d) Optical microscopy image of the twisted-pair-based stretchable low-pass filter (e) S-parameters of the stretchable low-pass filter at 0%, 20%, 25%, and 35% elongation plotted against frequency. Adapted from [14].

affected by the environment. The new design enables the RF electrodes to be utilized in thin-film bioelectronics, such as the epidermal electronic system (EES) [15]. Two fundamental RF characteristics of the scattering (S-) parameters determine the performance of the transmission lines: insertion loss representing S21 is the loss of power that results from an inserted device; return loss representing S11 is the loss of power in the signal returned or reflected. Figure 9(a) illustrates a unique design-concept of stretchable RF transmission line that is able to work at microwave frequencies with significantly low level of loss by integrating twisted-pair geometry into the serpentine shaped structures. Originally the design is inspired by the twisted-pair cabling from the telephone cables where the two conducting wires are twisted together. The balanced cable is well-known to minimize electromagnetic interference (EMI) from external surroundings. Figure 9(b) and (c) show the experimental results of the fabricated twisted-pair-based stretchable transmission line. For each line, the width was fixed to 25 μm and the thickness, via-hole size, and dielectric spacer thickness were optimized to be 1 μm, 150 μm$^2$, and 5 μm, respectively. Also, optical microscopy images of the transmission lines at different elongation are shown in Figure 10(b). The twisted-pair-based transmission lines presented remarkable performance with low insertion loss (about -1.1 dB at 40 GHz) and high return loss up to 40 GHz, which are attributed to the excellent confinement of the electromagnetic fields in the structure as well. To examine the effects during elongation, the transmission line was measured under different elongations (0%, 20%, 25%, and 35%) as shown in Figure 10(c). Almost negligible increases in insertion loss were observed with negligible performance change in return loss characteristics were observed as well.

In addition, the RF microwave filters are used to attenuate or transmit signals at certain frequency bands in microwave circuit. As an example of the application of the new design of RF transmission line, the low-pass filter presented in Figure 10(d) and the measured parameters are presented in Figure 10(e). The filter performed a wide band low-pass characteristic where the 3 dB cut-off frequency was 9.9 GHz, with a relatively flat band and low insertion loss between 11.6 GHz (-3.5 dB) and 15 GHz (-3.7 dB). The performance of the filter is slightly changed under stretched (0%, 20%, 25%, and 35% elongations) conditions. However, the capability to generate stretchable filters working at high frequency indicate potential of the new design of transmission line for stretchable microwave integrated circuits. Furthermore, the twisted-pair geometry can minimize interference with external noise, which would allow its operation on human skin. The design and fabrication represented in this work for stretchable transmission lines that operate at microwave frequencies are applicable in EES demanding wireless communication capabilities. Furthermore, stretchable microwave filters that is based on the twisted-pair structure promises potential of the twisted-pair-based transmission lines as passive components. This type of new transmission line is also suitable for high-speed digital circuits which requires minimized EMI from external environment. Integration of stretchable transmission lines with active devices, such as transistors and diodes to construct microwave integrated circuits remains one of the future challenges.

# 4. CONCLUSION

In summary, our group have been putting efforts to develop both high-frequency active and passive devices on flexible and stretchable substrates. Whereas most of the components developed were only demonstrated on flexible substrates such as plastic, these components can be connected using the stretchable transmission line developed on rubber substrates. The components can be formed into islands connected by serpentine transmission lines, so the strain is minimally affected on the devices during the stretching. It was shown that different semiconductor materials can be utilized to create flexible transistors working at extremely high frequencies. To integrate all the components into a circuits, other parameters such as the substrates' dielectric and thermal properties must be carefully considered as the frequency responses are highly sensitive to the intrinsic properties of the substrates. Typically, flexible and stretchable substrates comprised of organic materials have poor properties possessing low dielectric constant, low thermal conductivity, and high loss tangent compared to state-of-the-art substrates found in conventional RF chips and propose challenge to designing an RF circuit on them. Optimizations in substrates properties and fully integrating all the components by developing reliable integration technology into a circuit remains as a future challenge.

## REFERENCES

[1] Khang, D. Y., Jiang H., Huang Y. and Rogers J. A., "A stretchable form of single-crystal silicon for high-performance electronics on rubber substrates," Science 311(5758), 208-212 (2006).

[2] Meitl, M. A., Zhu Z.-T., Kumar V., Lee K. J., Feng X., Huang Y. Y., Adesida I., Nuzzo R. G. and Rogers J. A., "Transfer printing by kinetic control of adhesion to an elastomeric stamp," Nat. Mater. 5(1), 33-38 (2006).

[3] Jung, Y. H., Chang T.-H., Zhang H., Yao C., Zheng Q., Yang V. W., Mi H., Kim M., Cho S. J., Park D.-W., Jiang H., Lee J., Qiu Y., Zhou W., Cai Z., Gong S. and Ma Z., "High-performance green flexible electronics based on biodegradable cellulose nanofibril paper," Nat. Commun. 6, 7170 (2015).

[4] Hwang, S.-W., Tao H., Kim D.-H., Cheng H., Song J. K., Rill E., Brenckle M. A., Panilaitis B., Won S. M., Kim Y.-S., Song Y. M., Yu K. J., Ameen A., Li R., Su Y., Yang M., Kaplan D. L., Zakin M. R., Slepian M. J., Huang Y., Omenetto F. G. and Rogers J. A., "A physically transient form of silicon electronics," Science 337(6102), 1640-1644 (2012).

[5] Jung, Y. H., Zhang H., Cho S. J. and Ma Z., "Flexible and stretchable microwave microelectronic devices and circuits," IEEE Trans. Electron Devices PP(99), 1-13 (2017).

[6] Yuan, H.-C., Ma Z., Roberts M. M., Savage D. E. and Lagally M. G., "High-speed strained-single-crystal-silicon thin-film transistors on flexible polymers," J. Appl. Phys. 100(1), 013708 (2006).

[7] Zhou, H., Seo J.-H., Paskiewicz D. M., Zhu Y., Celler G. K., Voyles P. M., Zhou W., Lagally M. G. and Ma Z., "Fast flexible electronics with strained silicon nanomembranes," Sci. Rep. 3, 1291 (2013).

[8] Chang, T.-H., Xiong K., Park S. H., Mi H., Zhang H., Mikael S., Jung Y. H., Han J. and Ma Z., "High power fast flexible electronics: Transparent RF AIGaN/GaN HEMTs on plastic substrates," IEEE MTT-S Int. Microw. Symp. Dig. 1-4 (2015).

[9] Sun, L., Qin G., Huang H., Zhou H., Behdad N., Zhou W. and Ma Z., "Flexible high-frequency microwave inductors and capacitors integrated on a polyethylene terephthalate substrate," Appl. Phys. Lett. 96(1), 013509 (2010).

[10] Cho, S. J., Jung Y. H. and Ma Z., "X-band compatible flexible microwave inductors and capacitors on plastic substrate," IEEE J. Electron Devices 3(5), 435-439 (2015).

[11] Ma, Z., Jung Y. H., Seo J.-H., Chang T.-H., Cho S. J., Lee J., Zhang H. and Zhou W., "Materials and design considerations for fast flexible and stretchable electronics," IEDM Tech. Dig. Papers 19.2.1-19.2.4 (2015).

[12] Xu, S., Zhang Y., Cho J., Lee J., Huang X., Jia L., Fan J. A., Su Y., Su J., Zhang H., Cheng H., Lu B., Yu C., Chuang C., Kim T.-I., Song T., Shigeta K., Kang S., Dagdeviren C., Petrov I., Braun P. V., Huang Y., Paik U. and Rogers J. A., "Stretchable batteries with self-similar serpentine interconnects and integrated wireless recharging systems," Nat. Commun. 4, 1543 (2013).

[13] Zhang, Y., Xu S., Fu H. R., Lee J., Su J., Hwang K.-C., Rogers J. A. and Huang Y., "Buckling in serpentine microstructures and applications in elastomer-supported ultra-stretchable electronics with high areal coverage," Soft Matter 9(33), 8062-8070 (2013).

[14] Jung, Y. H., Lee J., Qiu Y., Cho N., Cho S. J., Zhang H., Lee S., Kim T. J., Gong S. and Ma Z., "Stretchable twisted-pair transmission lines for microwave frequency wearable dlectronics," Adv. Funct. Mater. 26(26), 4635-4642 (2016).

[15] Kim, D.-H., Lu N., Ma R., Kim Y.-S., Kim R.-H., Wang S., Wu J., Won S. M., Tao H., Islam A., Yu K. J., Kim T.-I., Chowdhury R., Ying M., Xu L., Li M., Chung H.-J., Keum H., McCormick M., Liu P., Zhang Y.-W., Omenetto F. G., Huang Y. G., Coleman T. and Rogers J. A., "Epidermal electronics," Science 333(6044), 838-843 (2011).